Journal of Thermal Science Vol.27, No.3 (2018) 203−212

https://doi.org/10.1007/s11630-018-1001-8 **Article ID: 1003-2169(2018)03-0203-10**

Thermal Modeling and Management of Solid Oxide Fuel Cells Operating with Internally Reformed Methane

WU Yiyang[1], SHI Yixiang[1*], CAI Ningsheng[1], NI Meng[2]

1. Key Laboratory for Thermal Science and Power Engineering of Ministry of Education, Tsinghua University, Beijing 100044, China

2. Building Energy Research Group, Department of Building and Real Estate, The Hong Kong Polytechnic University, Hung Hom, Kowloon, Hong Kong, 999077, China

Abstract: A detailed three-dimensional mechanistic model of a large-scale solid oxide fuel cell (SOFC) unit running on partially pre-reformed methane is developed. The model considers the coupling effects of chemical and electrochemical reactions, mass transport, momentum and heat transfer in the SOFC unit. After model validation, parametric simulations are conducted to investigate how the methane pre-reforming ratio affects the transport and electrochemistry of the SOFC unit. It is found that the methane steam reforming reaction has a "smoothing effect", which can achieve more uniform distributions of gas compositions, current density and temperature among the cell plane. In the case of 1500 W/m^2 power density output, adding 20% methane absorbs 50% of internal heat production inside the cell, reduces the maximum temperature difference inside the cell from 70 K to 22 K and reduces the cathode air supply by 75%, compared to the condition of completely pre-reforming of methane. Under specific operating conditions, the pre-reforming ratio of methane has an optimal range for obtaining a good temperature distribution and good cell performance.

Keywords: Solid Oxide Fuel Cell; Methane Steam Reforming; Modelling; Smoothing Effect; Pre-reforming Percentage

1. Introduction

The solid oxide fuel cell (SOFC) directly converts chemical energy to electrical energy with high efficiency and low pollution, which has promising applications in combined heat and power (CHP) units, auxiliary power units (APU) and distributed off-grid generator [1]. The high operating temperature (873-1273 K) of SOFC allows considerable flexibility of feed fuels (fossil fuel, natural gas, biogas and so on). Methane remains as the most interesting fuel for SOFC systems, for its abundance in natural gas and biogas [2]. As the electrochemical oxidation of CH_4 in SOFC anode is difficult, CH_4 fuel is usually utilized in SOFC indirectly via the steam reforming reaction either externally or internally. In most commercialized SOFC systems, methane is externally reformed to produce fuel gases containing hydrogen and carbon monoxide. Methane external reforming parameters can be adjusted easily to obtain desired gas composition and temperature to favor electrochemical reactions in SOFC [3]. However, strong exothermic effects of electrochemical reactions and various irreversibilities inside

Received: March 13, 2018 Corresponding author: SHI Yixiang, Professor; E-mail: shyx@mail.tsinghua.edu.cn
This study is financially supported by the National Natural Science Foundation of China (Grant No.51776108, No.51476092)

SOFC units tend to raise the temperature and cause a large temperature gradient in SOFC. Far excess air should flow through the cathode chamber to remove heat, which then reduces the system efficiency [4]. Since the methane steam reforming reaction (MSR) is a highly endothermic reaction with the potential to well absorb the generated heat inside SOFC, the internal reforming of methane has attracted much attention in recent years [5,6].

The internal steam reforming of methane faces several technical challenges. Firstly, the conventional anode material nickel is an effective hydrocarbon cracking catalyst, which has a high propensity for carbon deposition [7,8]. Carbon deposition at the anode side could lead to cell performance losses and poor durability. To minimize or eliminate coking, new anode materials have been developed, which showed good anti-coking performance in a short period but long-term behaviors remain to be studied. For practical applications, the use of high steam-to-carbon ratio (S/C) is required [9]. However, preheating the large amount of steam consumes lots of energy and a higher steam content in fuel will decrease the reversible cell voltage. Secondly, the high rate of steam reforming reaction in the anode inlet cools the inlet region a lot [10,11]. The steep temperature gradients resulted from the cooling effect could lead to significant thermal tensions, which in the worst case causes mechanical failure of the cells. To solve the problems of the tensions and large temperature gradients close to the inlet region and possible carbon formation, it is suggested that some degree of external pre-reforming of methane could be a promising way [12]. Although part of methane is reformed in the external reformer, the internal steam reforming reaction still takes place and carbon deposition could occur under certain conditions, such as insufficient steam in SOFC anode. A higher ratio of hydrogen to methane will decrease the rate of carbon formation [13]. Furthermore, carbon dioxide produced by partially pre-reforming is an effective coking inhibitor [14]. Considering the thermal management aspect, partially pre-reforming of methane increases the ratio of hydrogen to methane and narrows the gap between the reforming rate and electrochemical reaction rates, which mitigates the cooling effect close to the anode inlet region. A durability test of a SOFC stack with partially pre-reformed liquefied natural gas (LNG) shows a relatively uniform temperature distribution and undetectable carbon deposition [15], which demonstrates the potential of partially pre-reforming for SOFC applications.

To achieve a more uniform temperature distribution and inhibit carbon formation in SOFC with partially pre-reforming, the operating conditions including the gas composition at the inlet must be carefully controlled. The intercoupling of gas composition and heat between methane steam reforming and electrochemical reactions complicates the transport and reaction phenomena in the cell, especially in large SOFC cells or stacks, where ribs of the interconnector could substantially influence the gas transport under the ribs. Computational methods are currently recognized as dependable methods and are helpful to study the coupled phenomena [16]. Although some preliminary studies on SOFC with partially pre-reforming are available, they focus either on button cells or on a single SOFC channel, without considering the variation between different SOFC channels and the effects of the ribs [10, 17-18]. In this paper, a comprehensive 3D mechanistic model of a large-scale anode-supported SOFC unit with multiple gas channels is developed, considering the effect of the ribs. The model couples a validated electrochemical sub-model with heat and mass transfer for simulating a cell unit with real geometry. The differences between fully pre-reformed and partially pre-reformed methane are carefully evaluated. Finally, the impact of the pre-reforming percentage on SOFC performance is discussed.

2. Model development

2.1 Model geometry

A sketch of a planar SOFC unit is shown in Fig. 1. The detailed description and key geometry parameters of the unit can be found in our previous paper [19]. The following assumptions are made in this model:

(1) Steady state;

(2) All gas species are incompressible ideal gas;

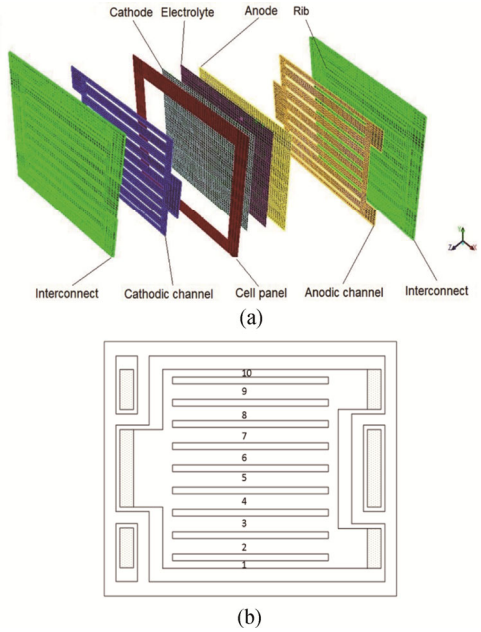

Fig. 1 A sketch of a planar SOFC unit (a) and the interconnector (b)

(3) The reaction active sites are uniformly distributed in the electrodes, and the ionic and electronic conductors are continuous and homogeneous;

(4) The flow in the gas channels and electrodes is laminar;

(5) 20% of heat generated inside the unit is released to the environment;

(6) Radiation heat exchange is neglected;

Governing equations—The governing equations include the methane pre-reforming reaction, charge-, mass-, momentum- and energy balance.

The methane reforming model adopts the dynamic model developed by Xu [20]. The reforming temperature is adjusted to achieve different methane pre-reforming ratios. Then, the partially pre-reformed fuel gas composition is set as the anode inlet gas. In this paper, the initial ratio of steam to methane is set as 2.

2.2 Charge conservation

The electronic and ionic charge balance at the electrodes and ionic charge balance at the electrolyte are listed in Table 1. The local transfer current density $i_{trans,\,an}$ and $i_{trans,\,ca}$ can be formulated as follows [16]:

$$i_{trans,an}=i_{trans,an,H_2}+i_{trans,an,CO} \tag{6}$$

$$i_{trans,\mathrm{ca}}=i_{trans,\mathrm{ca},H_2}+i_{trans,\mathrm{ca},CO} \tag{7}$$

The transfer current density can be calculated by generalized Butler-Volmer equation as follows:

$$i_{trans}=i_0\left(\frac{C_{react}}{C^*_{react}}\exp\left(\alpha\frac{n_eF\eta}{RT}\right)-\frac{C_{prod}}{C^*_{prod}}\exp\left(-(1-\alpha)\frac{n_eF\eta}{RT}\right)\right) \tag{8}$$

$C_{react}, C^*_{react}, C_{prod}, C^*_{prod}$ are the concentrations of reactants and products at reaction active sites and the electrode/channel interface, respectively. And i_0 stands for the exchange current density, which can be calculated as follows [21]:

$$i_{0,an,H_2}=\frac{\beta_{an,H_2}RT}{3F}\exp\left(-\frac{E_{act,an,H_2}}{RT}\right)\left(p_{O_2,an}\right)^{0.133} \tag{9}$$

$$i_{0,an,\mathrm{CO}}=\frac{\beta_{an,\mathrm{CO}}RT}{3F}\exp\left(-\frac{E_{act,an,\mathrm{CO}}}{RT}\right)\left(p_{O_2,an}\right)^{0.133} \tag{10}$$

$$i_{0,ca}=\frac{\beta_{ca}RT}{4F}\exp\left(-\frac{E_{act,\mathrm{ca}}}{RT}\right)\left(p_{O_2,ca}\right)^{0.25} \tag{11}$$

$\beta_{an,H_2}, \beta_{an,\mathrm{CO}}$ and β_{ca} denote the adjustable parameters for fitting the experimental data. It is reported that the electrochemical oxidation of H_2 is 1.9-2.3 times and 2.3-3.1 times higher than that of CO at 1023 K and 1273 K [22]. Therefore, β_{an,H_2} is assumed to be 2.5 times of $\beta_{an,CO}$.

Table 1 Governing equations for charge balance

Domain Ion conservation	Governing equations	
Anode	$-\nabla\cdot(\sigma^{eff}_{ion,an}\nabla V_{ion})=Q_{ion,an}=i_{trans,an}S_{TPB}$	(1)
Cathode	$-\nabla\cdot(\sigma^{eff}_{ion,\mathrm{ca}}\nabla V_{ion})=Q_{ion,\mathrm{ca}}=-i_{trans,\mathrm{ca}}S_{TPB}$	(2)
Electrolyte	$-\nabla\cdot(\sigma^{eff}_{ion,\mathrm{el}}\nabla V_{ion})=Q_{ion,\mathrm{el}}=0$	(3)
Electron conservation		
Anode	$-\nabla\cdot(\sigma^{eff}_{\mathrm{elec},an}\nabla V_{elec})=Q_{\mathrm{elec},an}=-i_{trans,an}S_{TPB}$	(4)
Cathode	$-\nabla\cdot(\sigma^{eff}_{\mathrm{elec,ca}}\nabla V_{elec})=Q_{\mathrm{elec,ca}}=i_{trans,\mathrm{ca}}S_{TPB}$	(5)

2.3 Mass conservation

The mass conservation domains include anode, cathode and gas channels, which are shown in Table 2. Chemical reactions in the gas channels are neglected in this model. In the anode, the mass sources from chemical reactions and electrochemical reactions are considered. The water gas shift reaction (WGSR) and steam reforming reaction are taken into consideration:

$$CH_4+H_2O\rightarrow 3H_2+CO\quad \Delta H^0_{298}=205.9\ kJ/mol \tag{20}$$

$$CO+H_2O\rightarrow H_2+CO_2\quad \Delta H^0_{298}=-41.1\ kJ/mol \tag{21}$$

The global expressions of the reactions kinetics are adopted from Haberman and Young's model [23].

Table 2 Mass conservation equations

Domain	Governing equations	
Anode	$\nabla\left(\rho_{fuel}\vec{v}x_i-\rho_{fuel}\omega_i\sum_{k=1}^{N}D^{eff}_{i,k}\nabla x_k\right)=R_i$	(12)
	$R_{H_2}=-\frac{i_{trans,an,H_2}S_{TPB}M_{H_2}}{2F}+r_{shift}M_{H_2}+3r_{refor\,\mathrm{ming}}M_{H_2}$	(13)
	$R_{H_2O}=\frac{i_{trans,an,H_2}S_{TPB}M_{H_2O}}{2F}-r_{shift}M_{H_2O}-r_{refor\,\mathrm{ming}}M_{H_2O}$	(14)
	$R_{CO}=-\frac{i_{trans,an,CO}S_{TPB}M_{CO}}{2F}-r_{shift}M_{CO}+r_{refor\,\mathrm{ming}}M_{CO}$	(15)
	$R_{CO_2}=\frac{i_{trans,an,CO}S_{TPB}M_{CO_2}}{2F}+r_{shift}M_{CO_2}$	(16)
	$R_{CH_4}=-r_{refor\,\mathrm{ming}}M_{CH_4}$	(17)
Cathode	$\nabla\left(\rho_{air}\vec{v}x_j-\rho_{air}\omega_j\sum_{k=1}^{N}D^{eff}_{j,k}\nabla x_k\right)=R_j$	(18)
	$R_{O_2}=\frac{i_{trans,\mathrm{ca}}S_{TPB}M_{O_2}}{4F}$	(19)

2.4 Momentum conservation

In gas channels, a laminar flow is described by the Navier-Stokes equation, and the flow in the porous electrodes is described by Darcy's law. The governing equations are listed in Table 3.

Energy conservation—The radiative heat transfer is

neglected in this model, therefore energy conservation equations are listed in Table 4.

Table 3 Momentum conservation equations

Domain	Governing equations	
Electrode	$\nabla\cdot\left(\varepsilon\rho_{gas}\vec{v}\vec{v}\right)=-\varepsilon\nabla p+\nabla\left[\varepsilon\mu_{gas}\left(\nabla\vec{v}+\left(\nabla\vec{v}\right)^{T}\right)\right]-\frac{\mu_{gas}}{\alpha}\varepsilon^{2}\vec{v}$	(22)
Gas channel	$\nabla\cdot\left(\rho_{gas}\vec{v}\vec{v}\right)=-\nabla p+\nabla\left[\mu_{gas}\left(\nabla\vec{v}+\left(\nabla\vec{v}\right)^{T}\right)\right]$	(23)

Table 4 Energy conservation equations

Domain	Governing equations	
Anode	$\nabla\cdot\left(-k\nabla T\right)=r_{shift}T\Delta S_{shift}+r_{reforming}T\Delta S_{reforming}+\frac{R_{H_2,an}T(S_{H_2O}-S_{H_2}-\frac{1}{2}S_{O_2})}{M_{H_2}}+\frac{R_{CO,an}T(S_{CO_2}-S_{CO}-\frac{1}{2}S_{O_2})}{M_{CO}}+\eta_{an,H_2}\left\|Q_{elec,an,H_2}\right\|+\eta_{an,CO}\left\|Q_{elec,an,CO}\right\|+\frac{i_{ion}^2}{\sigma_{an,ion}}+\frac{i_{elec}^2}{\sigma_{an,elec}}$	(24)
Cathode	$\nabla\cdot\left(-k\nabla T\right)=\eta_{ca}\left\|Q_{elec,ca}\right\|+\frac{i_{ion}^2}{\sigma_{an,ion}}+\frac{i_{elec}^2}{\sigma_{an,elec}}$	(25)
Electrolyte	$\nabla\cdot\left(-k\nabla T\right)=\frac{i_{ion}^2}{\sigma_{el,ion}}$	(26)
Interconnects	$\nabla\cdot\left(-k\nabla T\right)=\frac{i_{elec}^2}{\sigma_{interer,elec}}$	(27)
Gas channel	$\nabla\cdot\left(-k\nabla T+\vec{v}\cdot\rho c_p T\right)=0$	(28)

2.5 Model parameters

The model parameters including all the material properties are presented in the previous paper [19].

2.6 Model solution

The partial differential equations describing multi-physics field are solved with the finite volume method by the commercial software ANSYS Fluent™ (ANSYS, Inc., Canonsburg, PA, USA) [24]. The model is solved at a given cell voltage.

3. Results and Discussion

3.1 Model validation

Since the electrochemical reactions strongly influence the heat and mass distribution, parameters related to the electrochemical model should be validated to be reasonable. An electrochemical sub-model based on a button cell running on syngas is simulated and the results are compared with corresponding experimental data, as shown in Fig. 2. It can be seen that the simulated profiles under different temperatures and gas compositions match the experimental data well. This verified that the electrochemical sub-model is reliable under wide ranges of temperatures and gas compositions.

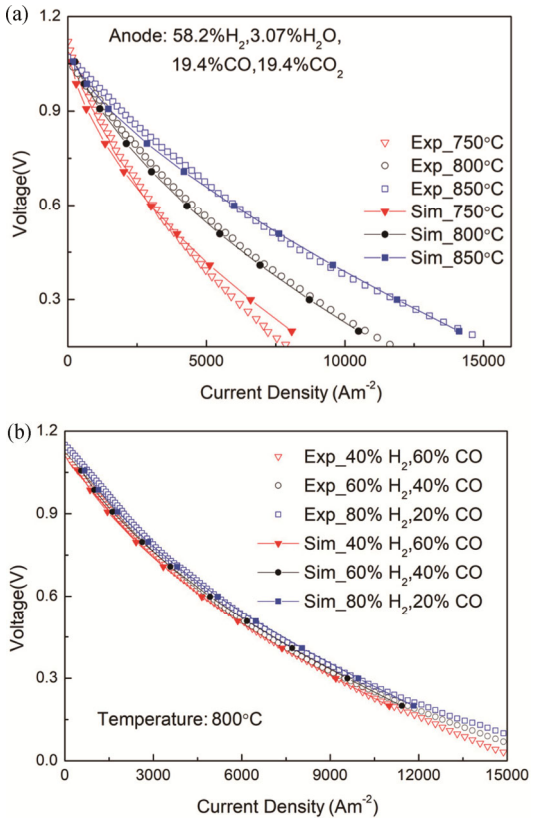

Fig. 2 Model validation under different temperatures (a) and different gas compositions (b)

3.2 Effects of methane internal reforming

The endothermic effect of methane steam reforming complicates the distributions of physical quantities in the SOFC unit. The cases with 100% pre-reformed (case A) and 36% pre-reformed (case B) methane as fuel gas are respectively discussed and compared. The operating conditions are listed in Table 5. The working voltage is set as 0.7 V.

Table 5 Operating conditions

Parameters	case A	case B
Pressure (Pa)	101325	101325
Fuel inlet temperature (K)	973	973
Air inlet temperature (K)	998	998
Fuel mole percentage	0.016% CH_4, 15.1% H_2O, 64.6% H_2, 14.9% CO, 5.24% CO_2	21.36% CH_4, 43.69% H_2O, 27.51% H_2, 1.18% CO, 6.26% CO_2
Fuel inlet flow rate (kg/s)	1.47e-6	1.47e-6
Air inlet flow rate (kg/s)	7.5e-5	2.625e-5

Fig. 3 presents the central velocity magnitude distributions in the anode gas channels. The two cases show different spatial distribution patterns. In case A, the highest velocity magnitude appears in the middle four channels, and the variations among the ten channels are relatively small. It shows the same distribution pattern with the case only considering the flow field. In case B, the velocity magnitude in the middle channels is the lowest, and the variation between channels is higher than that of case A. However, since the gas flow distances among the ten channels at the same x position are different, the velocity distribution pattern in case B is better for obtaining more uniform physical quantities distributions among the whole domain.

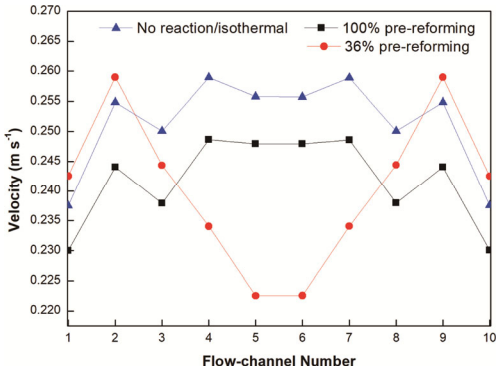

Fig. 3 Central velocity magnitude distributions in anodic channels

As H_2 and CO participate in the electrochemical reactions, the distributions of H_2 and CO in the anodic channel (as shown in Fig. 4) are important to the uniformity of current density and temperature distributions. In case A, concentrations of H_2 and CO decrease rapidly along the fuel flow direction, especially near the inlet region. Furthermore, the velocity distribution pattern results in an arcuate species distribution, which is uneven in the direction vertical to the flow direction. In case B, the molar fractions of H_2 and CO initially increase with increasing distance away from the inlet, and then decrease in the downstream of the cell. The different distributions of gas species between two cases are caused by the coupling effects between the electrochemical reactions and chemical reactions in case B. As the electrochemical reactions and methane steam reforming couple in the porous anode, both H_2 and CO are consumed by electrochemical oxidation but replenished by methane steam reforming. Therefore, the concentrations of H_2 and CO climb up first due to the significant methane steam reforming reaction and then decline along the flow direction due to low steam reforming rate in the downstream. The concentration distributions are more uniform both along and vertical to the flow direction.

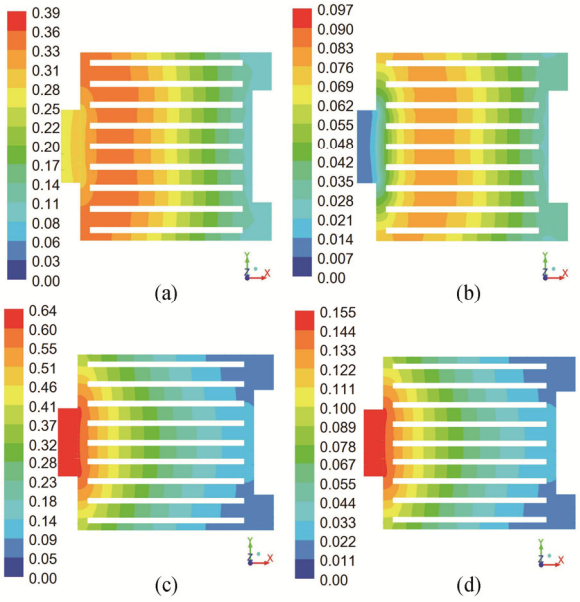

Fig. 4 Mole fraction of species distributions in the anodic channel: (a) H_2_case A-100% pre-reforming (b) H_2_case B-36% pre-reforming (c) CO_case A-100% pre-reforming (d) CO_case B-36% pre-reforming

Fig. 5 shows the current density distributions in the middle section of the electrolyte in both cases. The average current densities of case A and case B are 2326 A m^{-2} and 2172 A m^{-2}, respectively. Although the current densities are very close in both cases, the distributions are extremely different. In case A, the current density is the highest near the inlet and declines steeply along the flow direction, which explains the significant reductions in H_2/CO molar fractions near the inlet in Fig. 4(a) and 4(c). The current density near the anode outlet is only 20% of that at the anode inlet, which explains the relatively small variation in fuel concentration in the downstream in Fig. 4(a) and 4(c). And the arcuate distribution regularities also appear, indicating an obvious channel-to-channel variation. While in case B, the current density climbs up to reach a peak value, and then decreases along the flow direction. The increased current density in the upstream is caused by the increased fuel concentration by methane steam reforming (Fig. 4(b) and 4(d)). The maximum current density appears at one-third of the flow channel with its value being only 66% of that in case A. The variation of current density is smoothed obviously, for the reason that methane steam reforming redistributes the concentrations of H_2 and CO along the anodic channel. It should be noted that current densities under the ribs are substantially lower than those under the gas flow channels in both cases, owing to large oxygen diffusion resistance under the ribs of the porous cathode [25].

The uniformity of temperature distributions always remains a crucial problem in SOFC, as many failure be-

haviors are often caused by bad temperature distributions. The temperature distributions in the middle section of the electrolyte are shown in Fig. 6. In case A, excess air flows through the cathode channel to take away heat generated from fuel electrochemical reactions. It can be seen that the region near the cathode inlet is greatly cooled by the cooling air. The maximum temperature appears at the anode inlet, for the reason that electrochemical reactions are strongest here. The maximum temperature difference along the flow direction is 70 K. While in case B, owing to the cooling effect of methane steam reforming at the fuel inlet and cathodic air flux at the SOFC outlet, the maximum temperature appears in the middle position of the cell. The maximum temperature difference is reduced to 22 K. The cooling effect near the anode inlet region depends on the amount and the ratio of methane to hydrogen. Under the condition of completely internal steam reforming, a large local temperature gradient would appear in the fuel inlet region, while partially external reforming of methane avoids this area very well. The temperature distribution regularity in Fig. 6(b) agrees with the experiment results conducted on a 2.5 kW SOFC stack [15].

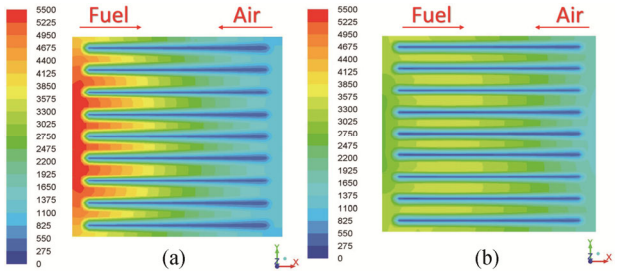

Fig. 5 Current density (Am^{-2}) distributions in the middle section of the electrolyte: (a) case A-100% pre-reforming and (b) case B-36% pre-reforming

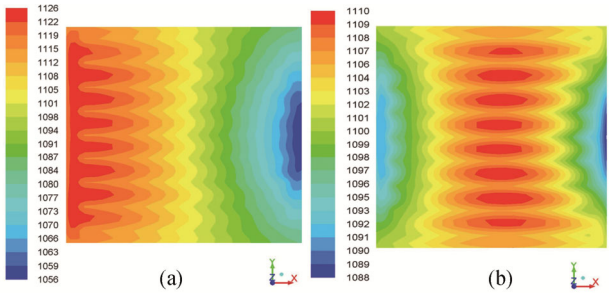

Fig. 6 Temperature (K) distributions in the middle section of the electrolyte: (a) case A-100% pre-reforming and (b) case B-36% pre-reforming

To better understand the effect of methane steam reforming, the total heat generation rates in cross-sections of positive electrode-electrolyte-negative electrode (PEN) perpendicular to the flow direction are shown in Fig. 7. The total heat generation includes fuel oxidation heat, water gas shift reaction and methane steam reforming heat, electrode polarization heat and ohmic heat. These four parts of heat generation distributions are depicted in Fig. 8. To make it clearer, all the data have been plotted in dimensionless form, by using the value of each property of the PEN as a reference. As shown in Fig. 7, the heat generation distributions are dominated by the electrochemical reactions in case A. The total heat generation rate decreases rapidly along the anode flow channel, and its value at the anode outlet is less than 30% of that at the anode inlet. While in case B, the variation of the total heat generation shows an opposite pattern compared to that in case A. At the anode inlet, the strong endothermic nature of methane steam reforming dominates and the total heat effect is endothermic. As fuels flow downstream, the electrochemical reactions start to dominate in heat generation, but the endothermic effect of methane steam reforming weakens the growing trend of total heat generation. Therefore, the total heat generation rate increases mildly along the anode flow direction. The heat generation rates of four contributing parts shown in Fig. 8 demonstrate this process more clearly. In case A, heat generation rates of all the four parts show the same variation trends along the anode flow direction. While in case B, the heat release from water-gas shift reaction and methane steam reforming decreases rapidly along the flow direction, due to the low concentration of CH_4 fuel. This indicates that methane is mainly reformed in the region close to the fuel inlet. The heat generation rates of other three parts represent uniform distributions along the flow direction.

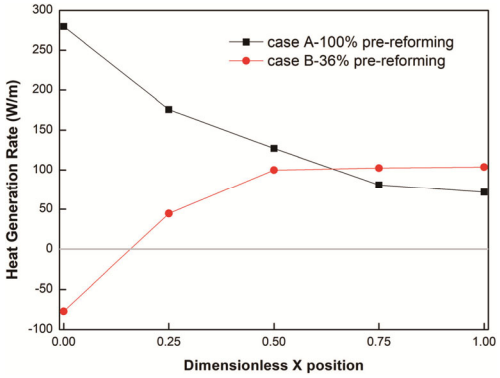

Fig. 7 Total heat generation rate in cross-sections of PEN perpendicular to the flow direction

To make a brief sum-up, using partially pre-reformed methane as the fuel gas shows comparable electrochemical output with that using completely pre-reformed methane. Furthermore, partial pre-reforming effectively reduces the non-uniformity of current density and temperature, which in turn decreases thermal tensions in the cell and help improve the durability.

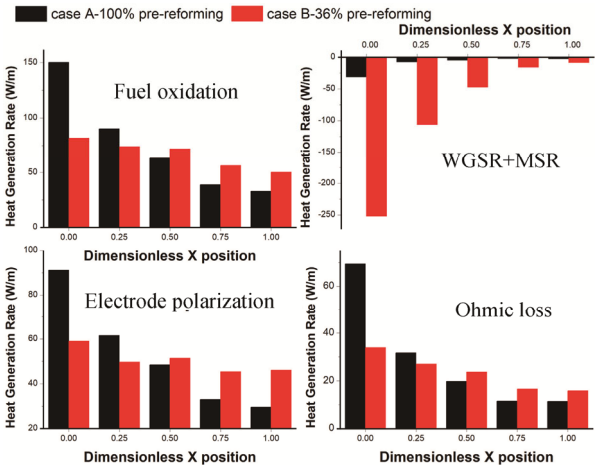

Fig. 8 Heat generation rate in cross-sections of PEN perpendicular to the flow direction

3.3 Effects of methane pre-reforming percentage

As stated before, temperature and current density distributions depend on the amount and ratio of methane to electrochemical active reactants (H_2 and CO). Therefore, the impact of methane pre-reforming percentage on cell performance is worthy of further study. For better comparison, all the operating conditions of different cases under different methane pre-reforming percentages are kept the same as that shown in Table 5, except that the cathode air fluxes are adjusted to obtain similar average temperatures of the fuel cell unit.

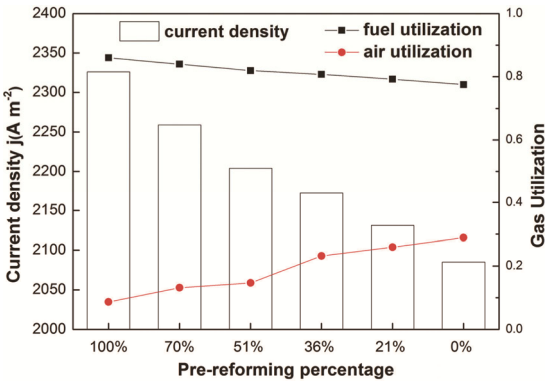

Fig. 9 Current density, fuel and air utilization under different methane pre-reforming percentages

Fig. 9 shows the current density, fuel and air utilization under different methane pre-reforming percentages. Under partially pre-reforming conditions, current density keeps decreasing when reducing the pre-reforming percentage. Current density under 0% pre-reforming is 11% lower than that under 100% pre-reforming. Since methane steam reforming reduces the total heat generation of the cell, the cathode air flux decreases with reducing the methane pre-reforming percentage. It can be seen that the air utilization rate under 0% pre-reforming case is up to 30%, while its value is less than 10% under 100% pre-reforming case.

Fig. 10 depicts total heat generation rates of PEN under different methane pre-reforming percentages. The overall length of the solid bar represents the total heat generation by exothermic reactions, and the length above the horizontal axis represents the net heat generation of PEN. It can be concluded that the lengths of solid bars under different cases are almost the same, which means that methane steam reforming does not affect the cumulative heat generation from electrochemical reactions. That is to say, the endothermic effect of methane steam reforming only does subtraction on the total heat generation. Another issue should be mentioned that the total heat generation cannot be offset entirely by methane steam reforming. Under the 0% pre-reforming case, the endothermic effect of methane steam reforming takes up 65% of the total heat generation.

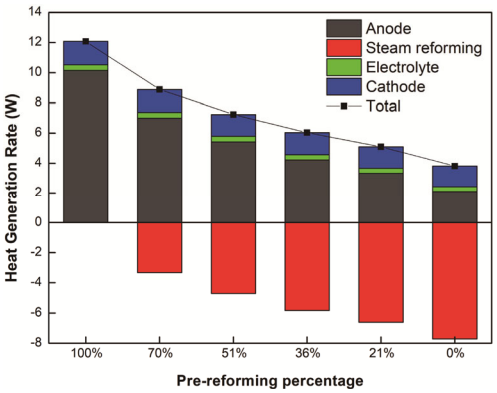

Fig. 10 The total heat generation rates of PEN under different methane pre-reforming percentages

Fig. 11(a) shows the maximum, average and minimum temperatures of PEN under different pre-reforming percentages. Owing to the initial rough estimation, the average temperatures of PEN under these conditions are all close to 1100 K. However, the temperature variation is minimum (only about 22 K) when the pre-reforming percentage is about 36%. For comparison, the temperature variation under 100% pre-reforming percentage and 0% pre-reforming percentage are over 80 K and 30 K, respectively. The results clearly demonstrate that the temperature uniformity in the SOFC could be greatly reduced by carefully controlling the pre-reforming percentage. Fig. 11(b) presents the positions along the fuel flow direction with the highest temperature and maximum net heat generation rates. It clearly shows that both positions move to the downstream of the anode with reducing methane pre-reforming percentages. And the position with the highest temperature always falls behind the position with the maximum net heat generation rate,

due to the cathode reverse flow bringing heat to the upstream of the anode.

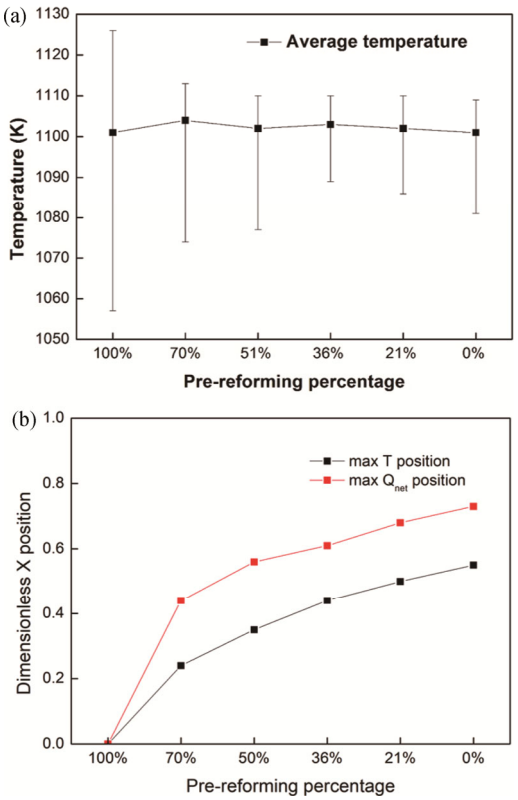

Fig. 11 (a) The maximum, average and minimum temperature of PEN (b) The positions with the maximum temperatures and net heat generation rates

To better understand the pre-reforming effect, the distributions of temperature and current density along the flow channels are shown in Fig. 12. The both ends of the middle channels (the channel 5, 6, as shown in Fig. 1(b)) face the anode inlet and cathode inlet respectively, so the differences of physical quantities along these two channels are the largest. Fig. 12 represents temperature and current density distributions along the flow channel in the channel 5, under different pre-reforming percentages. Under the 100% pre-reforming condition, the maximum temperature appears close to the anode inlet. By reducing pre-reforming percentage and the cathode air flux, temperature near the anode inlet decreases and temperature near the cathode inlet increases. Under the 70% and 51% pre-reforming conditions, the minimum temperatures still locate at the cathode inlet region. By reducing the pre-reforming percentage, the minimum temperature moves to the anode inlet region, and a small temperature drop appears within the first few millimeters of the anode length. The middle region always shows the maximum temperature, and reducing the pre-reforming percentage moves the maximum temperature downstream. Fig. 12(b) shows current density variations along the channel 5 under these conditions. Under the 100% pre-reforming condition, current density drops rapidly along the flow direction. In the other five pre-reforming conditions, the values and variation trends of current densities at the second half of the channels are almost the same. However, in the first half part, current densities keep decreasing with reducing pre-reforming percentages. This further indicates that methane is mostly reformed in the first half part of the cell. Under the 0% pre-reforming condition, current density at anode inlet is only 35% of that under the 100% pre-reforming condition and 45% of that under the 70% pre-reforming condition, respectively.

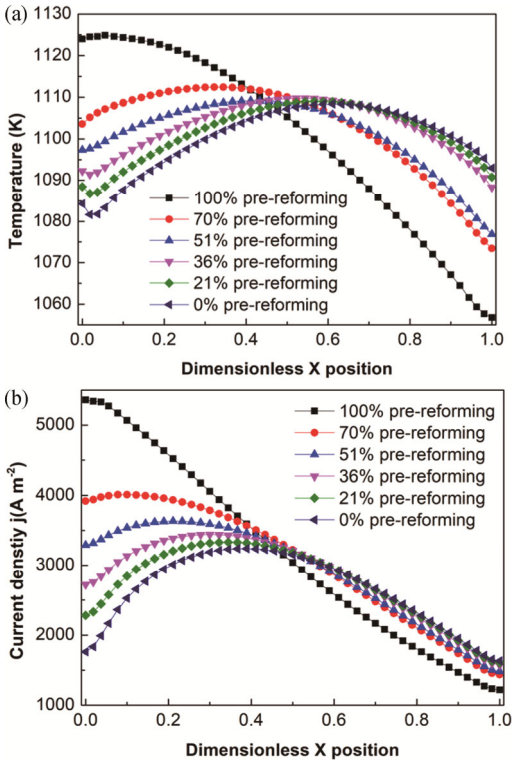

Fig. 12 Physical quantities distributions in flow-channel 5 along the flow direction: (a) temperature and (b) current density

The temperature uniformity along the flow direction is also an important indicator of an optimal temperature field. Fig. 13 represents the temperature uniformity in the central section of electrolyte under the middle line of ten flow channels (as shown in Fig. 1(b)). Each point shown in the figure represents the standard deviation of temperatures at 40 points equally distributed along a flow channel. The standard deviation under 100% pre-reforming condition is much larger than those under other conditions. The standard deviation decreases firstly and then increases with reducing pre-reforming percentages. Taking various factors into consideration, applying the pre-reforming percentage close to 36% can obtain better temperature uniformity.

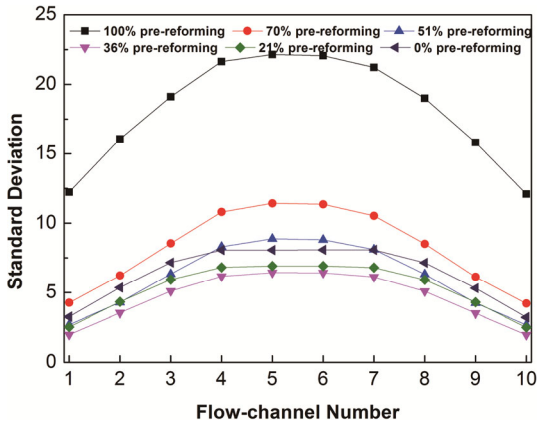

Fig. 13 Standard deviation of temperature along the flow direction in different channels

4. Conclusions

A comprehensive 3D mechanistic model of a large-scale planar SOFC unit running on partially pre-reformed methane is developed in this study. The model considers the coupling effect of chemical and electrochemical reactions, mass transport, momentum and heat transfer in the SOFC unit. Different from previous modeling studies on button cells or single-channeled SOFC cell, the present study fully considers the channel-to-channel variation. The electrochemical sub-model is validated with experimental data under different temperatures and gas compositions. The effect of partially pre-reformed methane is well presented and discussed. Part of conclusions are collected bellow:

The planar unit running on partially pre-reformed methane shows comparable cell performance with that running on entirely pre-reformed methane. The methane steam reforming reaction couples with electrochemical reactions both in terms of gas compositions and thermal effect, and it has a “smoothing effect” on the gas compositions, current density and temperature distributions among the cell unit.

The methane pre-preforming percentage has an evident effect on the cell performance. Reducing the pre-reforming percentage can substantially decrease the required cathode air flux, but lower the cell power density. There exists an optimal range of pre-reforming percentages for reducing the temperature non-uniformity.

Acknowledgement

Supports from the National Natural Science Foundation of China (51776108, 51476092) and Tsinghua University 221Youth Foundation Program for Fundamental Scientific Research are highly appreciated. This research is also supported by a grant from Environmental Conservation Fund of Hong Kong SAR (ECF 54/2015).

References

[1] Steele B. C. H., Heinzel A. Materials for fuel-cell technologies. Nature, 2001, 414(6861): 345–352.

[2] Gür T. M. Comprehensive review of me thane conversion in solid oxide fuel cells: Prospects for efficient electricity generation from natural gas. Progress in Energy and Combustion Science, 2016, 54: 1–64.

[3] Mueller F., Jabbari F., Gaynor R., Brouwer J. Novel solid oxide fuel cell system controller for rapid load following. Journal of Power Sources, 2007, 172(1): 308–323.

[4] Peters R., Riensche E., Cremer P. Pre-reforming of natural gas in solid oxide fuel-cell systems. Journal of Power Sources, 2000, 86(1-2): 432–441.

[5] Ni M., Leung D. Y. C., Leung M. K. H. Electrochemical modeling and parametric study of methane fed solid oxide fuel cells. Energy Conversion and Management, 2009, 50(2): 268–278.

[6] Klein J.M., Hénault M., Roux C., Bultel Y., Georges S. Direct methane solid oxide fuel cell working by gradual internal steam reforming: Analysis of operation. Journal of Power Sources, 2009, 193(1): 331–337.

[7] Bengaard H. S., Nørskov J. K., Sehested J., et al. Steam Reforming and Graphite Formation on Ni Catalysts. Journal of Catalysis, 2002, 209(2): 365–384.

[8] Iida T., Kawano M., Matsui T., Kikuchi R., Eguchi K. Internal reforming of SOFCs-Carbon deposition on fuel electrode and subsequent deterioration of cell. Journal of the Electrochemical Society, 2007, 154(2): B234–B241.

[9] Ahmed, K., Foger, K. Kinetics of internal steam reforming of methane on Ni/YSZ-based anodes for solid oxide fuel cells. Catalysis Today, 2000, 63(2-4): 479–487.

[10] Albrecht K. J., Braun R. J. The effect of coupled mass transport and internal reforming on modeling of solid oxide fuel cells part I: Channel-level model development and steady-state comparison. Journal of Power Sources, 2016, 304: 384–401.

[11] Kirtley J. D., Steinhurst D. A., Owrutsky J. C., Pomfret M. B., Walker R. A. In situ optical studies of methane and simulated biogas oxidation on high temperature solid oxide fuel cell anodes. Physical Chemistry Chemical Physics, 2014, 16(1): 227–236.

[12] Dicks A. L. Advances in catalysts for internal reforming in high temperature fuel cells. Journal of Power Sources, 1998, 71(1–2): 111–122.

[13] Kapicka J., Jaeger N. I., Schulzekloff G. Evidence for A hydrogen spillover effect in the deposition of coke on a nickel-faujasite catalyst during syngas conversion. Applied Catalysis a-General, 1992, 84(1): 47–55.

[14] Kirtley J., Singh A., Halat D., Oswell T., Hill J. M., Walker R. A. In Situ Raman Studies of Carbon Removal from High Temperature Ni-YSZ Cermet Anodes by Gas Phase Reforming Agents. The Journal of Physical Chemistry C, 2013, 117(49): 25908–25916.

[15] Fang Q., Blum L., Batfalsky P., Menzler N. H., Packbier U., Stolten D. Durability test and degradation behavior of a 2.5 kW SOFC stack with internal reforming of LNG. International Journal of Hydrogen Energy, 2013, 38(36): 16344–16353.

[16] Ahsan M., Hussain A. Computational Fluid Dynamics (CFD) Modeling of Heat Transfer in a Polymeric Membrane using Finite Volume Method. Journal of Thermal Science, 2016, 25 (6): 564–570.

[17] Ni M. Modeling of SOFC running on partially pre-reformed gas mixture. International Journal of Hydrogen Energy, 2012, 37(2): 1731–1745.

[18] Momma A., Takano K., Tanaka Y., Negishi A., Kato K., Nozaki K., Kato T., Ichigi T., Matsuda K., Ryu T. Internal reforming characteristics of cermet supported solid oxide fuel cell using yttria stabilized zirconia fed with partially reformed methane. Journal of Power Sources, 2009, 193(1): 65–71.

[19] Lin B., Shi Y., Ni M., Cai N. Numerical investigation on impacts on fuel velocity distribution nonuniformity among solid oxide fuel cell unit channels. International Journal of Hydrogen Energy, 2015, 40(7): 3035–3047.

[20] Xu J. G., Froment G. F. Methane steam reforming: II. diffusional limitations and reactor simulation. AICHE Journal, 1989, 35(1): 97–103.

[21] Nagata S., Momma A., Kato T., Kasuga Y. Numerical analysis of output characteristics of tubular SOFC with internal reformer. Journal of Power Sources, 2001, 101(1): 60–71.

[22] Matsuzaki Y., Yasuda I. Electrochemical oxidation of H_2 and CO in a H_2-H_2O-CO-CO_2 system at the interface of a Ni-YSZ cermet electrode and YSZ electrolyte. Journal of the Electrochemical Society, 2000, 147(5): 1630–1635.

[23] Haberman B. A., Young J. B. Three-dimensional simulation of chemically reacting gas flows in the porous support structure of an integrated-planar solid oxide fuel cell. International Journal of Heat and Mass Transfer, 2004, 47(17-18): 3617–3629.

[24] Makoto Y. Multi-Physics CFD Simulations in Engineering. Journal of Thermal Science, 2013, 22(4): 287–293.

[25] Kong W., Li J., Liu S., Lin Z. The influence of interconnect ribs on the performance of planar solid oxide fuel cell and formulae for optimal rib sizes. Journal of Power Sources, 2012, 204: 106–115.